Available online at www.sciencedirect.com
SCIENCE DIRECT
Journal of Sound and Vibration 294 (2006) 421–429
JOURNAL OF SOUND AND VIBRATION
www.elsevier.com/locate/jsvi

Discussion

Active structural acoustic control of a smart plate featuring piezoelectric actuators

Seung-Bok Choi*

Smart Structures and Systems Laboratory, Department of Mechanical Engineering, Inha University, Incheon 402-751, Republic of Korea

Received 15 February 2005; accepted 24 January 2006

Available online 11 April 2006

1. Introduction

Recently, the emergence of new actuator mechanisms associated with smart materials has triggered the development of active structural acoustic control strategy. These researches include electrorheological fluid [1], shape memory alloys [2] and piezoelectric materials [3–6]. The piezoelectric materials are widely used for structural vibration and noise control due to their merits in terms of low power consumption, lightweight, flexibility, wide dynamic range and fast response time. As well known, it is common to use the piezoelectric materials as sensors and actuators to make the structure to be smart.

In designing the piezoelectric active structures for noise or acoustic control, the optimal placement of the actuators is one of the most important factors to be considered. For example, Wang et al. [7] presented a formulation of the optimization problem for the placement of the piezoelectric actuators in adaptive least mean square (LMS) control systems. Varadan et al [8] studied the optimal placement of the disk-shaped piezoelectric actuators to reduce the radiated sound when excited by the acoustic pressure field. On the other hand, one of the most popular control techniques for active acoustic control of the piezoelectric-based smart plate is to employ the adaptive filtered-x LMS algorithm. In general, this method is very effective for low frequency noise control instead of high frequency noise. However, the robustness of the control system to parameter uncertainties such as the variation of natural frequency is not fully guaranteed.

Consequently, the main contribution of this research work is to present a robust control algorithm for active structural acoustic control system subjected to parameter uncertainties. In order to achieve this goal, a thin smart plate associated with the piezoelectric actuators is introduced and its governing model is derived and expressed by transfer function which consists of nominal and uncertain parts. After determining optimal placement of the piezoelectric actuators based on the minimization of the radiated sound power from the structure, a robust H_∞ controller is designed taking account for the variation of natural frequency and damping ratio as parameter uncertainties. The controller is realized through the microprocessor and control responses such as sound pressure are evaluated and presented in time domain.

*Tel.: +82 32 860 7319; fax: +82 32 868 1716.
E-mail address: seungbok@inha.ac.kr.

0022-460X/$ - see front matter
doi:10.1016/j.jsv.2006.01.040

2. Modeling and optimization

A simply supported rectangular plate where the piezoceramic patches are bonded to the top and bottom surfaces is considered as shown in Fig. 1. The plate is excited by a primary source and the piezoceramic actuators are used to control the sound radiating from the structure. The microphones located in the far field are arranged in a row across the central line of the plate in both the x and y directions. When the plate is thin and isotropic, by invoking the Hamilton's principle, the governing equation of motion for the displacement $w(x,y,t)$ and associated boundary conditions are obtained as follows [9]:

$$D_p \nabla^4 w + (\rho_p + \rho_{\mathrm{pe}}) \frac{\partial^2 w}{\partial t^2} = \frac{\partial^2 m_{xj}}{\partial x^2} + \frac{\partial^2 m_{yj}}{\partial y^2}, \tag{1}$$

$$w|_{x=0,a} = 0, \quad \frac{\partial^2 w}{\partial x^2} + v_p \frac{\partial^2 w}{\partial y^2}|_{x=0,a} = 0, \quad w|_{y=0,b} = 0, \quad \frac{\partial^2 w}{\partial y^2} + v_p \frac{\partial^2 w}{\partial x^2}|_{y=0,b} = 0, \tag{2}$$

$$D_{\mathrm{pe}} \left(\frac{\partial^2 w}{\partial x^2}(l_j, t) - c \cdot V(x,t) \right) = D_p \frac{\partial^2 w}{\partial x^2}(l_j, t), \quad j = 1, \ldots, 2N,$$

$$D_{pe} \left(\frac{\partial^2 w}{\partial y^2}(g_j, t) - c \cdot V(y,t) \right) = D_p \frac{\partial^2 w}{\partial y^2}(g_j, t), \quad j = 1, \ldots, 2N.$$

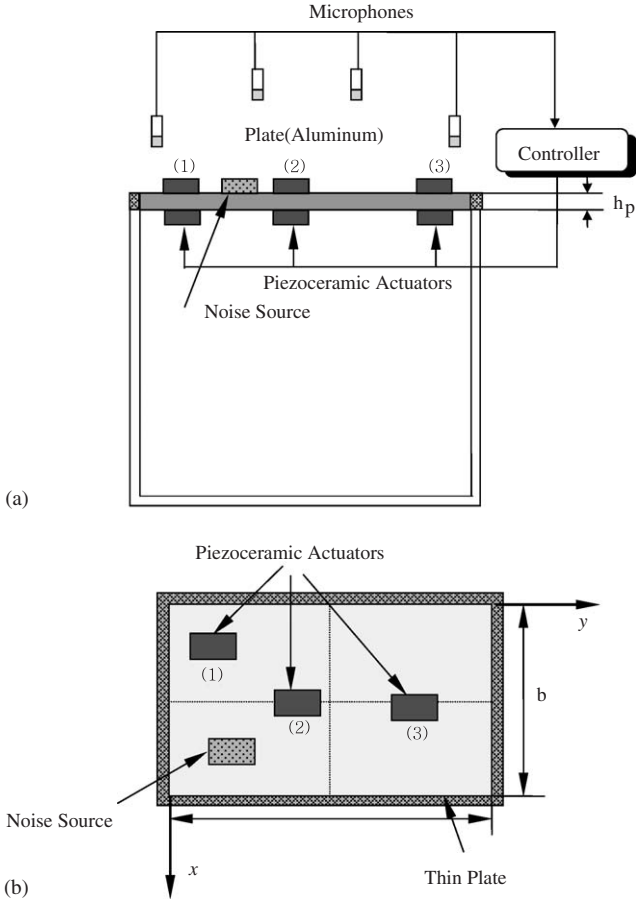

Fig. 1. Configuration of active structure-borne noise control system. (a) Schematic diagram, (b) top view.

In the above equation, D_p and D_{pe} is the bending stiffness of the plate and the piezoactuator, respectively, and ρ_p and ρ_{pe} is the density of the plate and the piezoactuator, respectively. m_{xj} and m_{yj} is the actuator-induced bending moment in the x and y direction, respectively. $V(x,t)$ and $V(y,t)$ is the control voltage applied to the x and y direction, respectively, and c is a constant that represents the bending moment per unit volt. Since Eq. (1) describes a linear distributed parameter system, control voltage $V(x,t)$ and $V(y,t)$ can be reduced to $V(t)$. Now, by introducing the ith modal coordinate $\eta_i(t)$ and ith mode eigenfunciton $\varphi_i(x,y)$, a decoupled ordinary differential equation for each mode is derived by

$$\ddot{\eta}_i + 2\zeta_i\omega_i\dot{\eta}_i + \omega_i^2\eta_i = D_p\frac{cV_j}{I_t}\int_{l_j}^{l_{j+1}}\int_{g_j}^{g_{j+1}}\left(\frac{\partial^2\varphi_i}{\partial x^2}+\frac{\partial^2\varphi_i}{\partial y^2}\right)\mathrm{d}x\,\mathrm{d}y,$$
$$i = 1,2,3,3,\ldots\infty, \quad j = 1,3,5,\ldots,2N-1, \tag{3}$$

where

$$I_t = \rho_p h_p\int_{l_j}^{l_{j+1}}\int_{g_j}^{g_{j+1}}\varphi_i^2\,\mathrm{d}x\,\mathrm{d}y.$$

In the above, ω_i is the natural frequency of the ith mode, ζ_i is the damping ratio of the ith mode, I_t is the generalized mass, and h_p is the thickness of the plate.

In order to obtain transfer function between the input voltage and the radiated sound pressure, the total sound pressure p_t can be expressed in the assumed mode method as follows:

$$p_t(R,\theta,\phi,x,y,t) = \sum_{i=1}^{n}\Omega_i(R,\theta,\phi,t)\varphi_i(x,y), \tag{4}$$

where

$$\Omega_i(R,\theta,\phi,t) = \chi(R,\theta,\phi)\eta_i(t).$$

In the above, $\Omega_i(R,\theta,\phi,t)$ is the modal value related to the ith mode. By taking a finite number of control modes (n mode), the overall transfer function is given by

$$G_j(s) = -\frac{c\cdot D_p\cdot\chi(R,\theta,\phi)\cdot\sum_{i=1}^{n}\varphi_i(a,b)\cdot\Gamma_{ji}/I_t}{\sum_{i=1}^{n}\left(s^2+2\zeta_i\omega_i s+\omega_i^2\right)}, \tag{5}$$

where

$$\Gamma_{ji} = \int_{l_j}^{l_{j+1}}\int_{g_j}^{g_{j+1}}\left(\frac{\partial^2\varphi_i}{\partial x^2}+\frac{\partial^2\varphi_i}{\partial y^2}\right)\mathrm{d}x\,\mathrm{d}y, \quad i = 1,2,3,\ldots,n \quad j = 1,3,5,\ldots,2N-1.$$

Before designing a controller, it is important to optimally design the location of the piezoactuators. This can be determined by minimizing the objective function given by

$$\Phi = \int_0^{2\pi}\int_0^{\frac{\pi}{2}}\frac{|p_t|^2}{2\rho c}r^2\sin\theta\,\mathrm{d}\theta\,\mathrm{d}\phi, \tag{6}$$

where, ρ is the density of the acoustic medium. The above function physically implies the integral of the mean squared sound pressure over a hemisphere of radius r in the far field [10]. In the design process, the actuator dimensions are fixed and only the location of the actuators is optimally searched. The actuator locations are sequentially searched. A set of microphones is assumed to measure the pressure field at the far field, because it reduces unnecessary spillover. In addition, one should recognize that the control voltage V_j is optimally adjusted when the location of the actuator is changed. In this work, the following aluminum plate and the piezoceramic actuator are used; for the aluminum; Young's modulus = 70 GPa, thickness = 1.2 mm, density = 2900 kg/m^3, width = 300 mm, length = 400 mm, and for the piezoceramic actuator; Young's modulus = 64 GPa, thickness = 1.0 mm, density = 7700 kg/m^3, width = 40 mm, length = 80 mm, strain constant = -30×10^{-10} (m/m)(N/m), stress constant = -5.6×10^{-3} (m/m)(N/m^2). Using these geometry and material properties, the first and second mode natural frequencies are evaluated by $\omega_i =$ 280 rad/s and

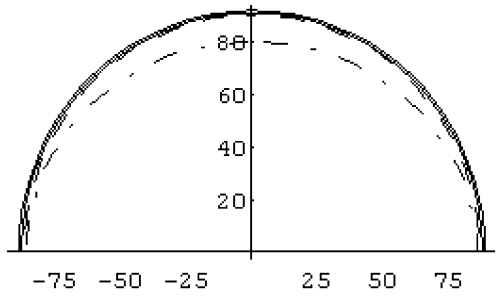

(a)

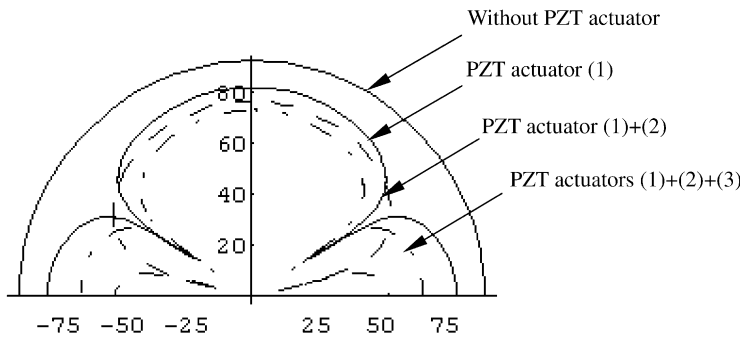

(b)

Fig. 2. Radiated directivity pattern ($\omega = 400$ rad/s). (a) Initial locations, (b) optimal locations.

$\omega_2 = 583$ rad/s, respectively. It is found that optimal locations of the actuator (1) is (0.123, 0.222), actuator (2) is (0.187, 0.149) and actuator (3) is (0.314, 0.102) at excitation frequency of 400 rad/s. Fig. 2 presents the radiated directivity pattern at the far field in $x-z$ plane for the optimally placed actuators and actuators at initial locations when excitation frequency is 400 rad/s. The results show that the optimally placed actuator provides much better reduction of sound radiation. Using the optimally chosen location of the piezoactuators a robust controller will be designed.

3. H_∞ controller design

The transfer function $G_1(s), G_2(s)$ and $G_3(s)$ corresponding to each piezoceramic actuator can be described by normalized left coprime factorization as follows:

$$G(s) = [G_1, G_2, G_3],$$

where

$$G_j(s) = -\frac{c \cdot D_p \cdot \chi(R,\theta,\phi) \cdot \sum_{i=1}^{2} \varphi_i(a,b) \cdot \Gamma_{ji}/I_t}{\sum_{i=1}^{2}\left(s^2 + 2\zeta_i\omega_i s + \omega_i^2\right)} = \tilde{M}_j^{-1}\tilde{N}_j, \quad j = 1,2,3. \tag{7}$$

Here the left coprime factorization $\left[\tilde{N}_j, \tilde{M}_j\right]$ of $G_j(s)$ is co-inner. On the other hand, the perturbed plant $G_{\Delta j}(s)$ with unstructured additive uncertainties on the normalized left coprime factors of the nominal plant $G_j(s)$ can be described as follows:

$$\begin{aligned} G_{\Delta j}(s) &= -\frac{c \cdot D_p \cdot \chi(R,\theta,\phi) \cdot \sum_{i=1}^{2} \varphi_i(a,b) \cdot \Gamma_{ji}/I_t}{\sum_{i=1}^{2}\left\{s^2 + 2(\zeta_i + \Delta\zeta_i)(\omega_i + \Delta\omega_i)s + (\omega_i + \Delta\omega_i)^2\right\}} \\ &= (\tilde{M}_j + \Delta_{M_j})^{-1}(\tilde{N}_j + \Delta_{N_j}) = \tilde{M}_{\Delta j}^{-1}\tilde{N}_{\Delta j}. \end{aligned} \tag{8}$$

In the above, $[\Delta_{N_j}, \Delta_{M_j}]$ represents the coprime factor uncertainties induced from the variations of system parameters such as natural frequencies and damping ratios of the smart plate. In this study, the parameter variation up to 20% of nominal values is considered. Fig. 3 presents the block-diagram of the proposed H_∞ control system. The control issue is to design the compensator $\mathbf{W}(s)$ and the feedback controller $\mathbf{K}_\infty(s)$. In order to guarantee the robust stability and performance of the proposed system, loop shaping is carried out using frequency-dependent pre-compensator $\mathbf{W}(s)$ ($=\text{diag}\{W_1, W_2, W_3\}$) until shaped plant $\mathbf{GW}$ satisfies the desired open loop shape. The inspection of the maximum singular value plot of the nominal plant indicates that considerable additional gain is required to minimize the effect of disturbance (pressure generated from noise source) on the plant output (sound pressure p_t). So suitable pre-compensators $W_1(s)$ (also, $W_2(s)$ and $W_3(s)$) are selected to ensure the robust stability of the proposed system. Fig. 4 shows singular value plot of the original plant G_1 and the shaped plant $G_1 W_1$. It is clearly seen that the gain has been much increased in the considered frequency range. This implies the increment of the robust stability. Next step is to find the optimal solution (γ_{opt}) to the normalized left coprime factor to guarantee robust stabilization of the shaped plant by following

$$\inf_{K_j} \left\| \begin{bmatrix} K_j \\ I \end{bmatrix} (I - G_{sj}K_j)^{-1} \tilde{M}_j^{-1} \right\|_\infty = \left\{ \sqrt{1 - \left\| \tilde{N}_{sj}, M_{sj} \right\|_H^2} \right\}^{-1} = \gamma_{\text{opt-j}}. \tag{9}$$

Here $\tilde{N}_{sj}$ and $\tilde{M}_{sj}$ denote the normalized left coprime factors of the shaped plant $\mathbf{G}_s(=[G_{s1}, G_{s2}, G_{s3}] = [G_1 W_1, G_2 W_2, G_3 W_3])$ and $\|\cdot\|_H$ denotes the Hankel norm. At this stage, γ_j can be viewed as a design indicator [11]: if the loop shaping has been well carried out, a sufficiently small value will be obtained for $\gamma_{\text{opt-j}}$.

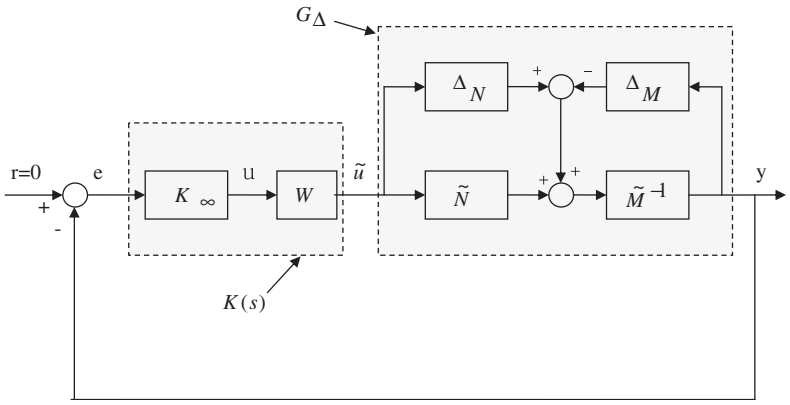

Fig. 3. Block-diagram of the H_∞ control system.

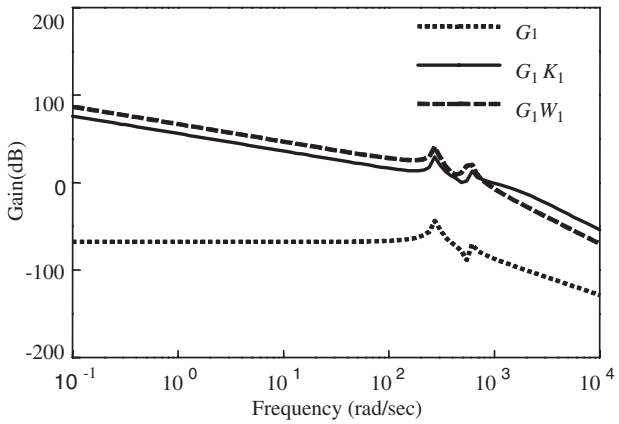

Fig. 4. Loop gain of the piezoactuator 1.

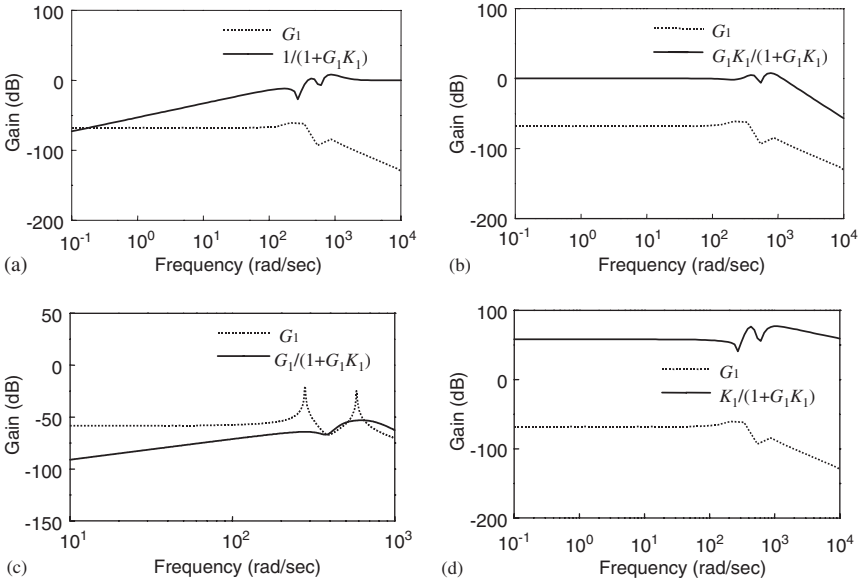

Fig. 5. Robust characteristics of the H_∞ control system. (a) Sensitivity transfer function, (b) complementary sensitivity transfer function, (c) singular value of controlled system, (d) control energy.

By choosing a suitable γ_j a little larger than $\gamma_{\text{opt}-j}$, $\gamma_1 = 4.7251$ was obtained in this work. The singular value plot of the loop gain G_1K_1 is presented in Fig. 4. As seen from the figure, the loop gain and the shaped plants are fairly well accorded with each other. This result means that the successful loop shaping has been achieved. In addition, Figs. 5(a) and (b) presents the sensitivity and complementary sensitivity function of the proposed system, respectively. It is seen from the sensitivity function plot that small magnitude in the low frequency region and 0 dB in the high frequency region are obtained. This result implies that the designed controller guarantees desired performance and it can reject the external disturbance effectively. Also from the complementary sensitivity function plot, it is seen that the sensor noise rejection is well guaranteed because small magnitude in the high frequency region and 0 dB in the low frequency region are obtained.

Now, by using previously obtained value of γ_j, we can constitute the sub-optimal controller $K_{\infty j}$ using the following state space formula [12]:

$$K_\infty = \left[\begin{array}{c|c} \dfrac{A_s^c + \gamma^2 W^{*-1} Z C_s^* (C_s^* + D_s F)}{B_s^* X} & \dfrac{\gamma^2 W^{*-1} Z C_s^*}{-D_s^*} \end{array}\right],$$
$$A_s^* = A_s + B_s F, \quad W = (XZ - \gamma^2 I) + I,$$
$$F = -S^{-1}(B_s^* X + D_s^* C_s), \quad S = I + D_s^* D_s. \tag{10}$$

Here (A_s,B_s,C_s,D_s) are the state space matrices of the shaped plant, and X and Z are the positive definite solutions of generalized control algebraic Riccati equation (GCARE) and generalized filtering algebraic Riccati equation (GFARE), respectively. Finally, combining it with the pre-compensators, the final H_∞ controllers are obtained as follows:

$$\mathbf{K} = \begin{bmatrix} K_1 & & \\ & K_2 & \\ & & K_3 \end{bmatrix} = \begin{bmatrix} W_1 K_{\infty 1} & & \\ & W_2 K_{\infty 2} & \\ & & W_3 K_{\infty 3} \end{bmatrix}. \tag{11}$$

The singular values of controlled (closed loop) system and control energy are presented in Figs. 5(c) and (a), respectively. From Fig. 5(c), it is seen that the proposed system can fairly reject the external disturbances such as pressure generated from the noise source.

4. Results and discussions

In order to demonstrate the effectiveness of the proposed control system an experimental investigation is undertaken. The smart plate is excited by the piezoelectric actuator and the sound signals are measured via the microphones and fed back to the microprocessor. An appropriate control voltage is determined for each actuator on the basis of the proposed H_∞ controller. The detailed numerical form of the controller is in Ref. [9]. The sampling frequency for the controller implementation is chosen by 1000 Hz.

Fig. 6 presents control responses under sinusoidal excitation with frequency of 400 rad/s. It is clearly observed that the imposed excitation has been well controlled by activating the controllers in both without and with uncertainties. It is noted that in the presence of the uncertainties control voltage has been increased in order to compensate the parameter variation. Fig. 7 presents control responses under random excitation. Again, it is obviously observed that the imposed excitation has been well suppressed by applying control voltage. This result directly indicates that control robustness to the parameter variations such as the variation of the natural frequency can be successfully achieved by employing the proposed H_∞ controller. Fig. 8 compares the control performance between the adaptive filter-x LMS method and the proposed H_∞ controller. In both cases, the imposed excitations have been well controlled, but the H_∞ controller shows less chattering in the settled phase and faster response than the filter-x LMS control algorithm.

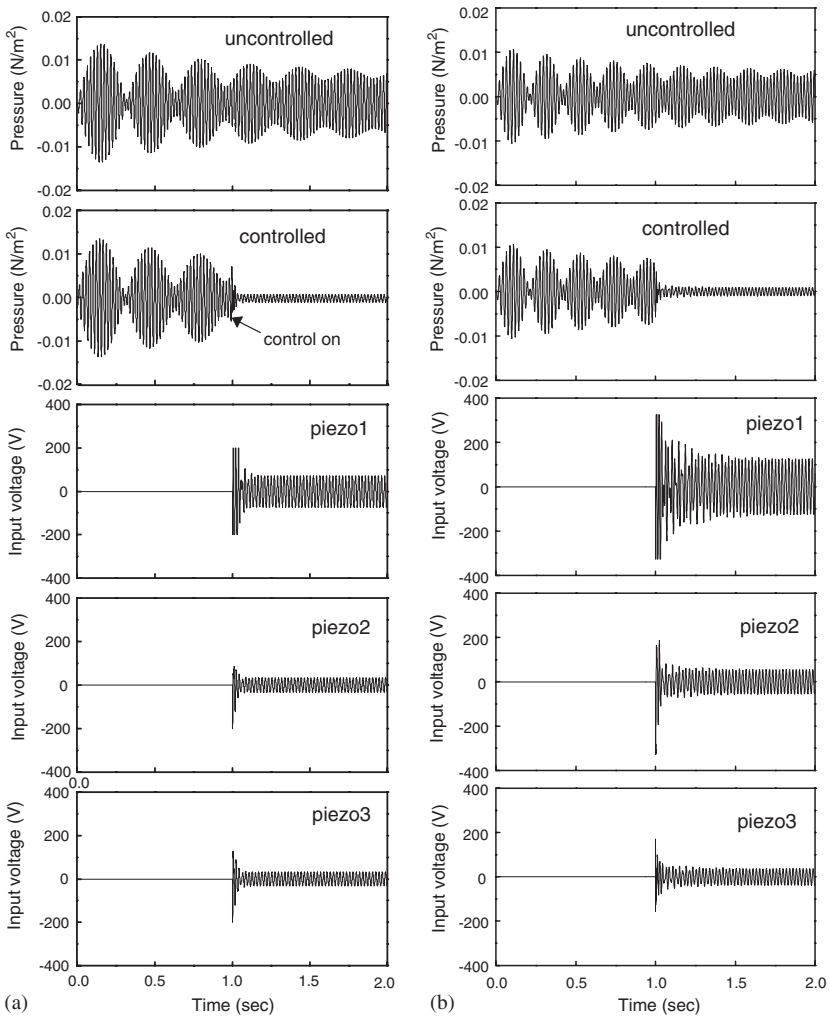

Fig. 6. Control responses under sinusoidal excitation: (a) w/o uncertainity, (b) with uncertainity.

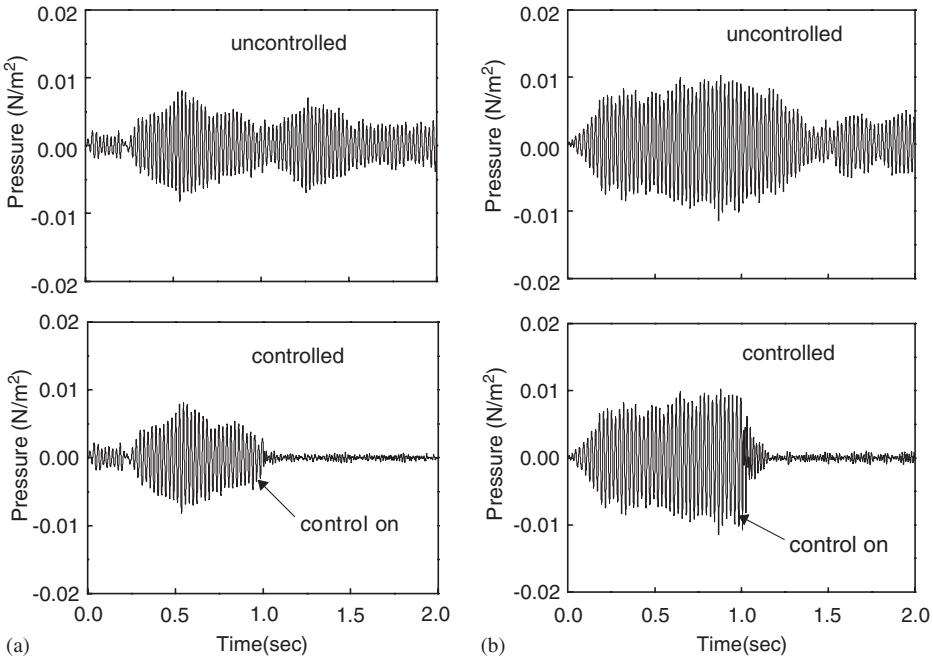

Fig. 7. Control responses under random excitation: (a) w/o uncertainity, (b) with uncertainity.

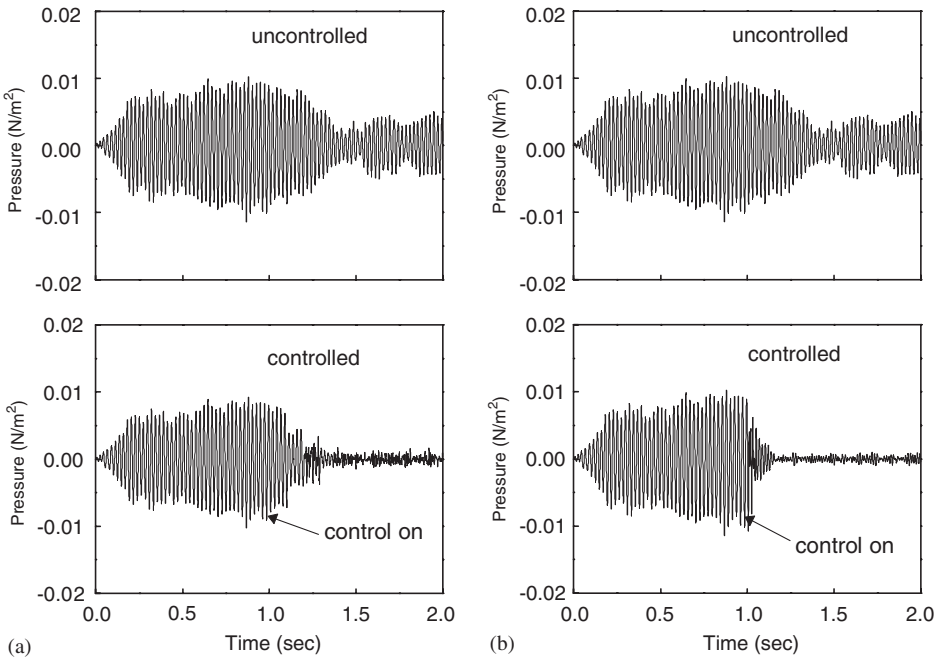

Fig. 8. Comparison of the control responses in the presence of the uncertainty. (a) Filtered-x LMS, (b) H_∞ controller.

5. Conclusion

A robust control for the structure-borne noise of a smart plate was undertaken by adopting the piezoelectric actuators. After formulating transfer function which relates the control input and the radiated sound output,

a robust H_∞ controller has been designed in the frequency domain. It has been demonstrated that the sound pressure under sinusoidal and random excitation can be substantially suppressed by activating the piezoelectric actuators associated with the robust controller. It has been also shown that the proposed H_∞ controller is very robust to the system uncertainties such as the variation of the natural frequency.

Acknowledgement

This work was supported by Inha University Research Grant. This financial support is gratefully acknowledged.

References

[1] S.B. Choi, S.W. Seo, J.H. Kim, K.S. Kim, An electrorheological fluid-based plate for noise reduction in a cabin: experimental results, *Journal of Sound and Vibration* 239 (1) (2001) 178–185.
[2] C.A. Rogers, Active vibration and structural acoustic control of shape memory alloy hybrid composites: experimental results, *Journal of Acoustical Society of America* 88 (6) (1990) 2803–2811.
[3] E.F. Crawley, Javier de Luis, Use of piezoelectric actuators as element of intelligent structures, *AIAA Journal* 25 (10) (1987) 1373–1385.
[4] L. Robert, C.R. Fuller, Experiments on active control of structurally radiated sound using multiple piezoceramic actuators, *Journal of Acoustical Society of America* 91 (6) (1992) 3313–3320.
[5] B.T. Wang, C.R. Fuller, R.A. Burdisso, Optimal placement of piezoelectric actuators for active structural acoustic control, *Journal of Intelligent Material Systems and Structures* 5 (1994) 67–76.
[6] J.H. Kim, V.V. Varadan, V.K. Varadan, Finite element optimization methods for the active control of radiated sound from a plate structure, *Smart Materials and Structures* 4 (4) (1995) 318–326.
[7] B.-T. Wang, R.A. Burdisso, C.R. Fuller, Optimal placement of piezoelectric actuators for active structural acoustic control, *Journal of Intelligent Material Systems and Structures* 5 (1994) 67–77.
[8] V.V. Varadan, J. Kim, V.K. Varadan, Optimal placement of piezoelectric actuators for active noise control, *AIAA Journal* 35 (3) (1997) 526–533.
[9] J.K. Lee, Active Structural Acoustic Control of Flexible Plate Structures Using Piezoceramic Actuators, Master Thesis, University of INHA, 1997.
[10] L.A. Roussos, Noise transmission loss of a rectangular in an infinite baffle, NASA Technical Paper 2398 (1985) 1–33.
[11] D.C. MacFarlane, K. Glover, A loop shaping design procedure using H_∞ synthesis, *IEEE Transactions on Automatic Control* 37 (6) (1992) 759–769.
[12] D.C. MacFarlane, K. Glover, *Robust Controller Design Using Normalized Coprime Factor Plant Descriptions*, Lecture Notes in Control and Information Sciences, Heidelberg, 1990.